

Supplementary Information:  
**UV Photodissociation Dynamics of the Acetone Oxide Criegee Intermediate:  
Experiment and Theory**

Guanghan Wang,<sup>1†</sup> Tianlin Liu,<sup>1†</sup> Meijun Zou,<sup>1</sup> Tolga N. V. Karsili,<sup>2,\*</sup> and Marsha I. Lester<sup>1,\*</sup>

<sup>1</sup> Department of Chemistry, University of Pennsylvania, Philadelphia, PA 19104-6323 USA

<sup>2</sup> Department of Chemistry, University of Louisiana at Lafayette, Lafayette, LA 70504 USA

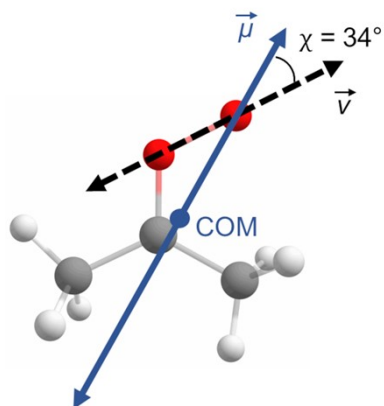
**Contents**

Scheme S1. Theoretical prediction of anisotropy parameter for (CH <sub>3</sub> ) <sub>2</sub> COO photodissociation.....	S2
Figure S1. Active orbitals used in CASSCF/CASPT2 calculations .....	S3
Figure S2. Comparison of jet-cooled action spectrum and thermal absorption spectra of (CH <sub>3</sub> ) <sub>2</sub> COO.....	S4
Figure S3. O ( <sup>1</sup> D) VMI images and resultant TKER distributions of (CH <sub>3</sub> ) <sub>2</sub> COO .....	S5
Figure S4. Optimized geometries of three Criegee intermediates and their co-products.....	S6
Figure S5. Illustration of selected normal modes of three Criegee intermediates.....	S7
Figure S6. Comparison between experimental and simulated TKER distributions for (CH <sub>3</sub> ) <sub>2</sub> COO .....	S8
Section SA. TKER simulation for <i>syn</i> -CH <sub>3</sub> CHOO .....	S9
Figure S7. Comparison between experimental and simulated TKER distributions for <i>syn</i> -CH <sub>3</sub> CHOO.....	S9
Table S1. Comparison between geometries optimized with different methods .....	S10
Table S2. VEEs of three Criegee intermediates .....	S11
Table S3. Properties of TKER distributions of three Criegee intermediates.....	S12
Table S4. Most changed coordinates in photodissociation.....	S13

---

<sup>†</sup> Equal contributions.

\* Corresponding author emails: [milester@sas.upenn.edu](mailto:milester@sas.upenn.edu), [tolga.karsili@louisiana.edu](mailto:tolga.karsili@louisiana.edu)



Scheme S1. Illustration of the calculated transition dipole moment ( $\vec{\mu}$ ) vector with origin at the center-of-mass (COM) of  $(\text{CH}_3)_2\text{COO}$ , photofragment recoil velocity vector ( $\vec{v}$ ) along the O-O bond axis, and the angle ( $\chi$ ) between them. In the molecular frame, the anisotropy parameter  $\beta$  is related to  $\vec{\mu}$ ,  $\vec{v}$ , and  $\chi$  via  $\beta = 2\langle P_2(\hat{\mu} \cdot \hat{v}) \rangle = 2\langle P_2(\cos \chi) \rangle$  where  $P_2$  is a second-order Legendre polynomial.<sup>1,2</sup> This yields a transition dipole moment at  $\chi = 34^\circ$  relative to the O-O bond, corresponding to  $\beta \sim 1.1$ , which is consistent with the experimental determination of  $\beta \sim 0.9\text{-}1.0$  (0.2) (Table S3). The transition dipole moment is computed using CASSCF(10,8)/aug-cc-pVTZ level of theory.

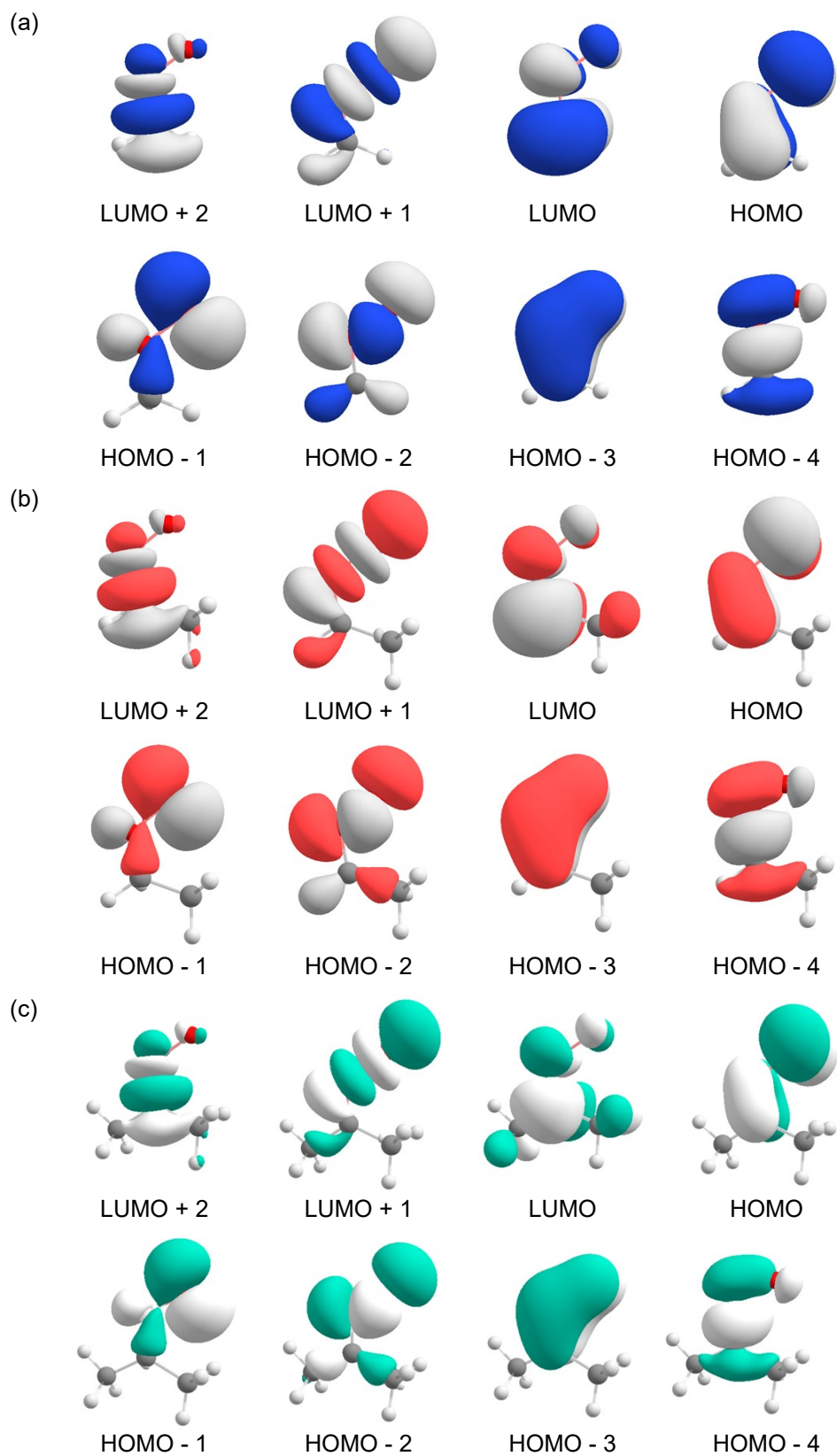


Figure S1. Active orbitals used in the CASSCF/CASPT2 computations for (a)  $\text{CH}_2\text{OO}$ , (b) *syn*- $\text{CH}_3\text{CHOO}$ , and (c)  $(\text{CH}_3)_2\text{COO}$ .

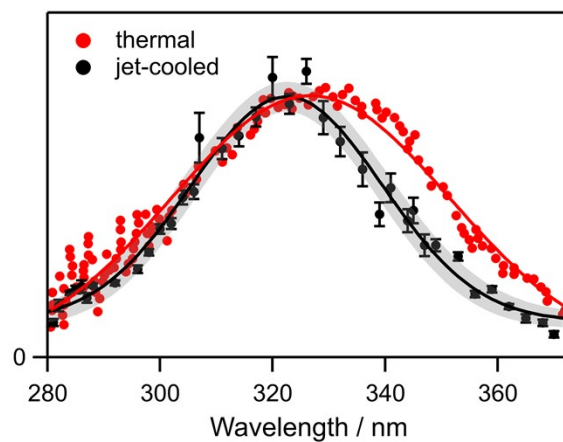


Figure S2. UV action spectrum of (CH<sub>3</sub>)<sub>2</sub>COO recorded under jet-cooled condition with O (<sup>1</sup>D) detection by 2+1 REMPI is compared with the previously reported direct absorption spectrum utilizing at transient absorption spectroscopy under thermal conditions (298 K, 100 torr). The solid lines through experimental data points are fits using a Gaussian lineshape. The thermal absorption spectrum is reproduced with permission from Ref. 3.

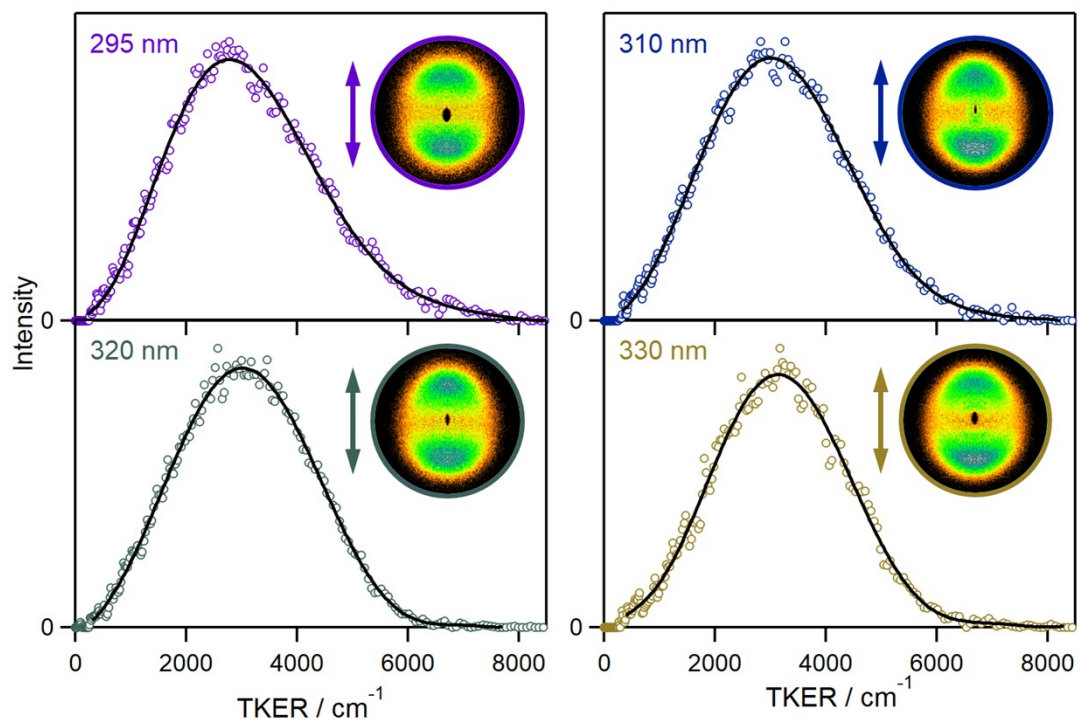


Figure S3. Total kinetic energy release (TKER) distributions (open circles) obtained by velocity map imaging of O (<sup>1</sup>D) products following UV excitation of (CH<sub>3</sub>)<sub>2</sub>COO at 295 nm, 310 nm, 320 nm and 330 nm. The TKER distributions for the O (<sup>1</sup>D) + (CH<sub>3</sub>)<sub>2</sub>CO (S<sub>0</sub>) product channel are fit with polynomial functions to guide the eye (black lines). Insets are the corresponding raw images (symmetrized) of the O (<sup>1</sup>D) products. The double-headed arrows represent the polarization of the UV radiation.

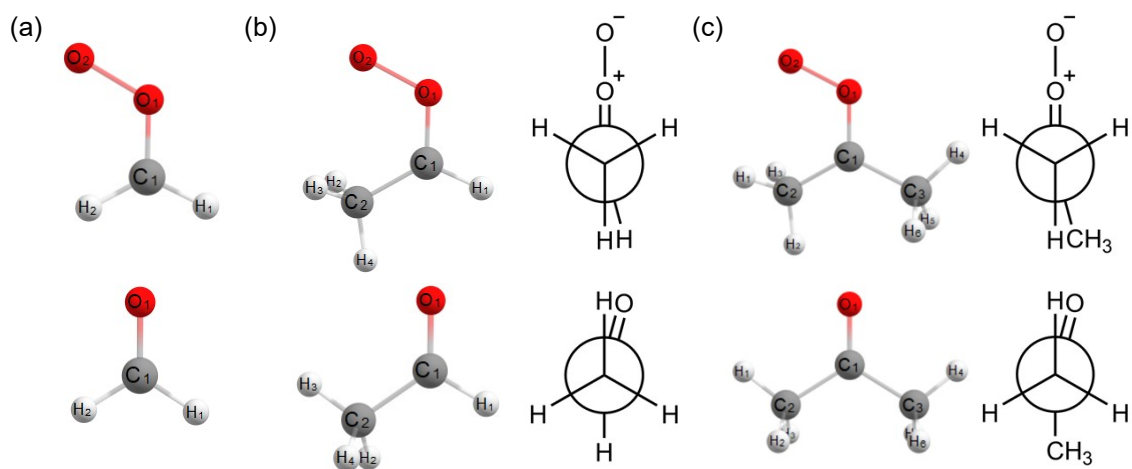


Figure S4. Ground state minimum geometries of (a)  $\text{CH}_2\text{OO}$ , (b) *syn*- $\text{CH}_3\text{CHOO}$ , and (c)  $(\text{CH}_3)_2\text{COO}$  and their corresponding aldehyde/ketone co-products, namely  $\text{H}_2\text{CO}$ ,  $\text{CH}_3\text{CHO}$ , and  $(\text{CH}_3)_2\text{CO}$ . The Newman projections along the  $\text{C}_1\text{C}_2$  bond are shown for the molecules in panel (b) and (c).

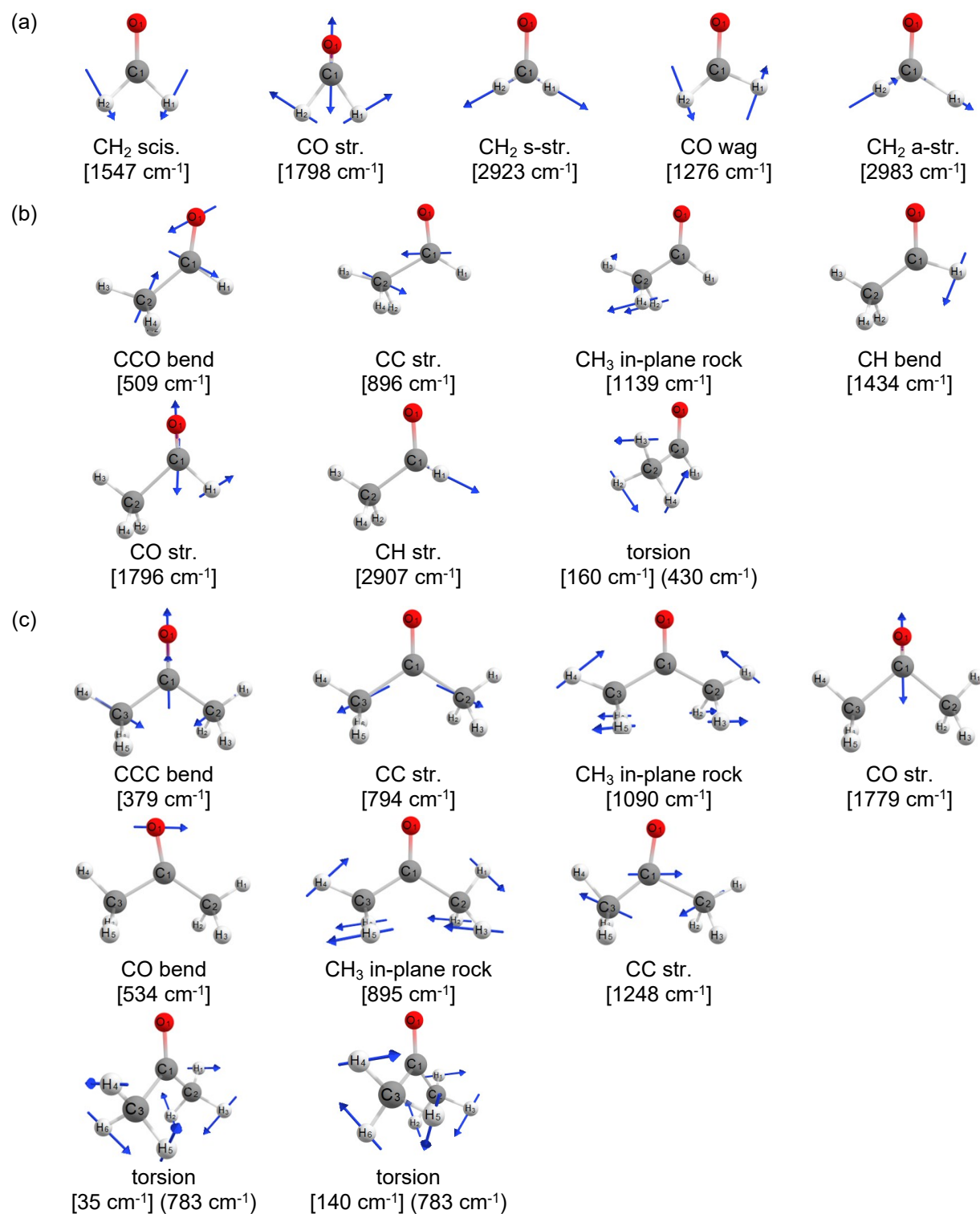


Figure S5. Illustration of the force vectors for the normal modes associated with the coordinates listed in Table S4 for (a) H<sub>2</sub>CO, (b) CH<sub>3</sub>CHO, and (c) (CH<sub>3</sub>)<sub>2</sub>CO. The corresponding harmonic frequencies (cm<sup>-1</sup>) are shown in brackets. In Panel (b) and (c), the torsional barriers obtained by relaxed scans are shown in parenthesis, and the symmetry number is 3 for the torsional potentials. The frequencies and torsional barriers are computed at the B2PLYP-D3/cc-pVTZ level of theory. The density of vibrational states are evaluated using Multiwell 2021,<sup>4</sup> which treats the methyl substituents as hindered rotors.

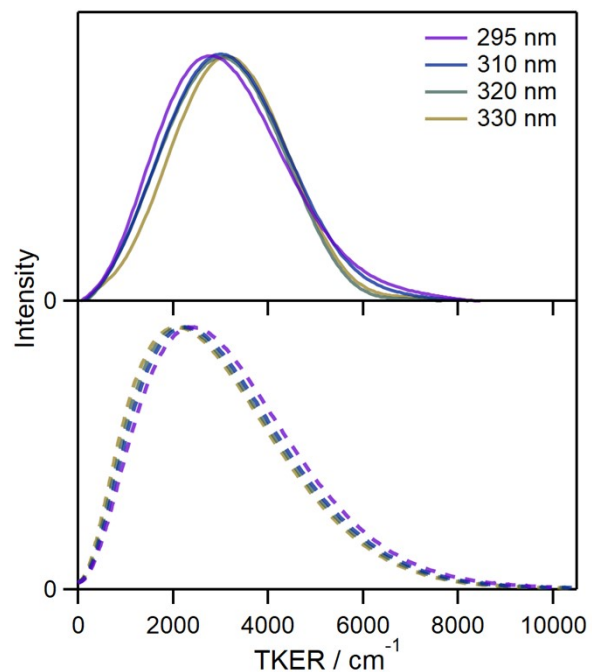


Figure S6. (Top) Summary of the TKER distributions (polynomial fits) obtained by VMI of O (<sup>1</sup>D) products following photodissociation of (CH<sub>3</sub>)<sub>2</sub>COO at different excitation wavelengths. (Bottom) Simulated TKER distributions for (CH<sub>3</sub>)<sub>2</sub>COO at the same excitation energies using a hybrid model that combines the reduced impulsive model with a statistical component, the latter component ranging from 15 to 35% with increasing excitation energies.

## Section SA. TKER simulation for *syn*-CH<sub>3</sub>CHOO

A hybrid model that combines the impulsive model with a statistical component is used to simulate the observed TKER distribution. The vibrational modes included in the impulsive model are shown in Figure S5, which are identified based on geometric changes from *syn*-CH<sub>3</sub>CHOO to CH<sub>3</sub>CHO (Table S4). Specifically, the C<sub>(1)</sub>O double bond is compressed by 0.07 Å, and the single bonds connecting the carbonyl C-atom with the H-atom and the methyl substituent are elongated by 0.03 and 0.04 Å, respectively, leading to activation in CO stretch, C<sub>(1)</sub>H stretch and C<sub>(1)</sub>C<sub>(2)</sub> stretch. The H<sub>(1)</sub>C<sub>(1)</sub>O and C<sub>(2)</sub>C<sub>(1)</sub>O angles are enlarged by 7° and 4°, respectively, corresponding to C<sub>(1)</sub>H bend and C<sub>(2)</sub>C<sub>(1)</sub>O bend vibrational excitation. In addition, the *syn*-methyl substituent in the CH<sub>3</sub>CHO is rotated by ca. 60° compared to the parent Criegee intermediate (Figure S4), and results in significant hindered rotational excitation of this methyl group, along with vibrational activation of the methyl in-plane rock. Again, overall rotational excitation of the CH<sub>3</sub>CHO product is neglected in the simulations. The statistical component accounting for 10% - 40% of the available energy brings the simulated TKER distributions for excitation wavelengths at 350 – 305 nm into good accord with experiment, shown in Figure S7. The resultant simulated TKER distributions are slightly broadened and shifted to higher TKER side with increasing excitation energy, agreeing with the increase in  $\langle \text{TKER} \rangle$  and FWHM derived from experiment.

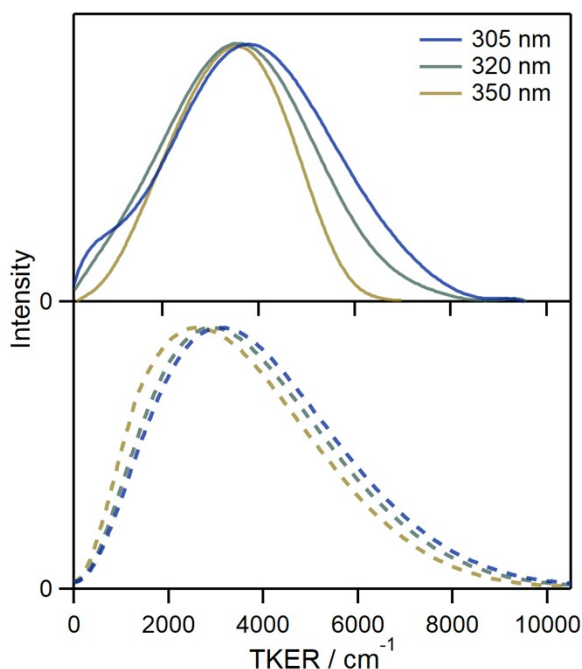


Figure S7. (Top) Reanalysis (polynomial fits) of the TKER data from Ref. 3 obtained by VMI of O (<sup>1</sup>D) products following photodissociation of CH<sub>3</sub>CHOO at different excitation wavelengths. (Bottom) Simulated TKER distributions for *syn*-CH<sub>3</sub>CHOO at the same excitation energies using a hybrid model that combines the reduced impulsive model with a statistical component, the latter component ranging from 10 to 40% with increasing excitation energies.

Table S1. Comparison of the optimized geometries (Z-matrix) obtained for (left) aldehyde/ketone ( $S_0$ ) product and (right) Criegee intermediate represented at long O-O distance, aldehyde/ketone---O ( $S_0$ ) at 4.0 Å, using B2PLYPD3/cc-pVTZ level of theory. The listed bond distances or angles are in the unit of Angstrom (Å) or degree (°).

H <sub>2</sub> CO ( $S_0$ )						H <sub>2</sub> CO---O ( $S_0$ )					
O						O					
O						O 1	4.000				
C 1	1.204					C 1	1.204	2	119.4		
H 2	1.103	1	122.1			H 3	1.103	1	122.1	2	178.9
H 2	1.103	1	122.1	3	180.0	H 3	1.103	1	122.1	2	358.9
CH <sub>3</sub> CHO ( $S_0$ )						CH <sub>3</sub> CHO---O ( $S_0$ )					
O						O					
O						O 1	4.000				
C 1	1.207					C 2	1.208	1	117.2		
C 2	1.500	1	124.6			C 3	1.500	2	124.5	1	360.0
H 2	1.107	1	120.3	3	180.0	H 3	1.107	2	120.3	1	180.0
H 3	1.091	2	109.5	1	238.4	H 4	1.091	3	109.5	2	238.4
H 3	1.086	2	110.6	1	0.0	H 4	1.086	3	110.6	2	0.0
H 3	1.091	2	109.5	1	121.6	H 4	1.091	3	109.5	2	121.7
(CH <sub>3</sub> ) <sub>2</sub> CO ( $S_0$ )						(CH <sub>3</sub> ) <sub>2</sub> CO---O ( $S_0$ )					
O						O					
O						O 1	4.000				
C 1	1.213					C 1	1.213	2	117.3		
C 2	1.511	1	121.8			C 3	1.511	1	121.8	2	180.1
C 2	1.511	1	121.8	3	180.0	C 3	1.511	1	121.7	2	0.1
H 3	1.085	2	109.9	1	360.0	H 4	1.085	3	110.0	1	360.0
H 3	1.091	2	110.1	1	238.8	H 4	1.090	3	110.1	1	238.8
H 3	1.091	2	110.1	1	121.2	H 4	1.090	3	110.1	1	121.1
H 4	1.085	2	109.9	1	0.0	H 5	1.085	3	110.0	1	360.0
H 4	1.091	2	110.1	1	238.8	H 5	1.091	3	110.1	1	238.8
H 4	1.091	2	110.1	1	121.2	H 5	1.091	3	110.1	1	121.1

Table S2. Vertical excitation energies (VEE, eV), corresponding wavelengths ( $\lambda$ , nm), and oscillator strengths ( $f$ ) for promotion of CH<sub>2</sub>OO, *syn*-CH<sub>3</sub>CHOO, and (CH<sub>3</sub>)<sub>2</sub>COO to their lowest six singlet excited states evaluated using the CASPT2(10,8)/aug-cc-pVTZ//B2PLYP-D3/cc-pVTZ method. The transitions predicted with strong oscillator strengths are highlighted in bold.

CH <sub>2</sub> OO		<i>syn</i> -CH <sub>3</sub> CHOO		(CH <sub>3</sub> ) <sub>2</sub> COO	
VEE / eV ( $\lambda$ / nm)	$f$	VEE / eV ( $\lambda$ / nm)	$f$	VEE / eV ( $\lambda$ / nm)	$f$
2.34 (529)	0.000	2.65 (468)	0.000	2.81 (442)	0.000
<b>3.87 (320)</b>	<b>0.103</b>	<b>3.98 (312)</b>	<b>0.102</b>	<b>3.97 (312)</b>	<b>0.124</b>
7.53 (165)	0.001	6.96 (178)	0.001	6.72 (184)	0.002
7.53 (165)	0.000	7.17 (173)	0.000	6.91 (179)	0.000
7.88 (157)	0.001	7.97 (156)	0.000	7.47 (166)	0.001
9.21 (135)	0.092	9.92 (125)	0.000	9.87 (126)	0.000

Table S3. Properties of the total kinetic energy release (TKER) and angular ( $\beta$ ) distributions derived from velocity map images of O ( $^1D$ ) products following UV excitation of  $CH_2OO$ ,  $CH_3CHOO$ , and  $(CH_3)_2COO$ , and the percentage of energy modeled as statistical component in the hybrid model.

Criegee Intermediate	$\lambda$ (nm)	$E_{avl}$ ( $cm^{-1}$ )	$E_{stat}$ (%)	$\langle TKER \rangle_1$ ( $cm^{-1}$ )	$FWHM_1$ ( $cm^{-1}$ )	$\frac{E_{int,1}}{E_{avl}}$ (%)	$\beta^f$	$\langle TKER \rangle_2$ ( $cm^{-1}$ )	TKER <sub>2</sub> contrib. <sup>g</sup> (%)
$CH_2OO^a$	310	15120 <sup>d</sup>	-	6570	5430	57	-	3840	23(3)
	320	14110 <sup>d</sup>	-	6150	5470	56	-	2640	12(1)
	330	13170 <sup>d</sup>	-	5800	5520	56	-	2290	11(1)
	340	12270 <sup>d</sup>	-	5200	4980	58	-	2000	10(1)
	350	11430 <sup>d</sup>	-	4660	4260	59	-	2480	22(3)
<i>syn</i> - $CH_3CHOO^b$	305	13980 <sup>e</sup>	40	3930	4000	72	0.8(1)	-	-
	320	12440 <sup>e</sup>	30	3660	3600	71	0.9(1)	-	-
	350 <sup>c</sup>	9760 <sup>e</sup>	10	3420	3500	65	0.8(1)	-	-
$(CH_3)_2COO$	295	14960 <sup>e</sup>	35	2840	3150	81	1.0(1)	-	-
	310	13320 <sup>e</sup>	30	2910	2990	78	0.9(2)	-	-
	320	12310 <sup>e</sup>	20	2830	2850	77	1.0(2)	-	-
	330	11360 <sup>e</sup>	15	2980	2630	74	0.9(2)	-	-

<sup>a</sup> Adapted from Ref. <sup>5</sup>.

<sup>b</sup> Adapted from Ref. <sup>6</sup>.

<sup>c</sup> Potential contribution from *anti*- $CH_3CHOO$  conformer at 350 nm.

<sup>d</sup> Experimentally determined dissociation energy from Ref. <sup>6</sup>.

<sup>e</sup> Re-evaluated with the calculated dissociation energies in this study.

<sup>f</sup> Average  $\beta$  and standard deviation ( $\pm 1\sigma$ ) derived from the FWHM region of each TKER distribution.

The recoil anisotropy is parallel, which implies that the transition dipole moment vector associated with  $S_2 \leftarrow S_0$  is parallel to the velocity vector (along O-O bond).

<sup>g</sup> Standard deviations ( $\pm 1\sigma$ ) derived from the fits.

Table S4. Ground state minimum geometry comparison between CH<sub>2</sub>OO, *syn*-CH<sub>3</sub>CHOO, (CH<sub>3</sub>)<sub>2</sub>COO and their corresponding aldehyde/ketone co-products regarding the coordinates with the most significant changes. Geometries were optimized with the B2PLYP-D3/cc-pVTZ level of theory.

	Bond Length (Å)			Angle (°)			Dihedral Angle (°)
	C <sub>(1)</sub> O <sub>(1)</sub>	C <sub>(1)</sub> H <sub>(1)</sub>	C <sub>(1)</sub> H <sub>(2)</sub>	H <sub>(1)</sub> C <sub>(1)</sub> O <sub>(1)</sub>	H <sub>(2)</sub> C <sub>(1)</sub> O <sub>(1)</sub>	-	-
CH <sub>2</sub> OO	1.270	1.077	1.080	115.0	118.8	-	-
CH <sub>2</sub> O	1.204	1.103	1.103	122.1	122.1	-	-
Diff.	-0.066	0.026	0.023	7.1	3.3	-	-
	C <sub>(1)</sub> O <sub>(1)</sub>	C <sub>(1)</sub> H <sub>(1)</sub>	C <sub>(1)</sub> C <sub>(2)</sub>	H <sub>(1)</sub> C <sub>(1)</sub> O <sub>(1)</sub>	C <sub>(2)</sub> C <sub>(1)</sub> O <sub>(1)</sub>	H <sub>(4)</sub> C <sub>(2)</sub> C <sub>(1)</sub>	H <sub>(3)</sub> C <sub>(2)</sub> C <sub>(1)</sub> O <sub>(1)</sub>
<i>syn</i> -CH <sub>3</sub> CHOO	1.273	1.080	1.465	113.0	120.8	111.5	-56.8
CH <sub>3</sub> CHO	1.207	1.107	1.500	120.3	124.6	109.5	0.0
Diff.	-0.065	0.027	0.035	7.3	3.9	-2.0	56.8
	C <sub>(1)</sub> O <sub>(1)</sub>	C <sub>(1)</sub> C <sub>(3)</sub>	C <sub>(1)</sub> C <sub>(2)</sub>	C <sub>(3)</sub> C <sub>(1)</sub> O <sub>(1)</sub>	C <sub>(2)</sub> C <sub>(1)</sub> O <sub>(1)</sub>	H <sub>(2)</sub> C <sub>(2)</sub> C <sub>(1)</sub>	H <sub>(1)</sub> C <sub>(2)</sub> C <sub>(1)</sub> O <sub>(1)</sub>
(CH <sub>3</sub> ) <sub>2</sub> COO	1.274	1.483	1.470	116.0	118.8	111.7	-56.5
(CH <sub>3</sub> ) <sub>2</sub> CO	1.213	1.511	1.511	121.8	121.8	110.1	0.0
Diff.	-0.061	0.028	0.041	5.8	3.0	-1.6	56.5

## References

1. B. J. Whitaker, *Imaging in Molecular Dynamics: Technology and Applications*, Cambridge University Press, Cambridge, 2003.
2. R. N. Zare, *Mol. Photochem.*, 1972, **4**, 1-37.
3. H. L. Huang, W. Chao and J. J. M. Lin, *Proc. Natl. Acad. Sci.*, 2015, **112**, 10857-10862.
4. J. R. Barker, T. L. Nguyen, J. F. Stanton, C. Aieta, M. Ceotto, F. Gabas, T. J. D. Kumar, C. G. L. Li, L. L. Lohr, A. Maranzana, N. F. Ortiz, J. M. Preses, J. M. Simmie, J. A. Sonk, and P. J. Stimac; MultiWell-2021 Software Suite; J. R. Barker, University of Michigan, Ann Arbor, Michigan, USA, Jan 2021; <https://multiwell.engin.umich.edu>.
5. V. J. Esposito, T. Liu, G. Wang, A. Caracciolo, M. F. Vansco, B. Marchetti, T. N. V. Karsili and M. I. Lester, *J. Phys. Chem. A*, 2021, **125**, 6571-6579.
6. H. Li, Y. Fang, N. M. Kidwell, J. M. Beames and M. I. Lester, *J. Phys. Chem. A*, 2015, **119**, 8328-8337.